Acta Crystallographica Section F
Structural Biology and Crystallization Communications
ISSN 1744-3091

Production, purification, crystallization and preliminary X-ray analysis of adeno-associated virus serotype 8

Michael Douglas Lane,[a] Hyun-Joo Nam,[a] Eric Padron,[a] Brittney Gurda-Whitaker,[a] Eric Kohlbrenner,[b] George Aslanidi,[b] Barry Byrne,[c] Robert McKenna,[a] Nicholas Muzyczka,[c] Sergei Zolotukhin[b] and Mavis Agbandje-McKenna[a]*

[a]Department of Biochemistry and Molecular Biology, Center for Structural Biology, McKnight Brain Institute, University of Florida, Gainesville, FL 32610, USA, [b]Division of Cell and Molecular Therapy, University of Florida, Gainesville, FL 32610, USA, and [c]Department of Molecular Genetics and Microbiology and Powell Gene Therapy Center, College of Medicine, University of Florida, Gainesville, FL 32610, USA

Correspondence e-mail: mckenna@ufl.edu

Received 16 March 2005
Accepted 3 May 2005
Online 1 June 2005

Adeno-associated viruses (AAVs) are actively being developed for clinical gene-therapy applications and the efficiencies of the vectors could be significantly improved by a detailed understanding of their viral capsid structures and the structural determinants of their tissue-transduction interactions. AAV8 is ~80% identical to the more widely studied AAV2, but its liver-transduction efficiency is significantly greater than that of AAV2 and other serotypes. The production, purification, crystallization and preliminary X-ray crystallographic analysis of AAV8 viral capsids are reported. The crystals diffract X-rays to 3.0 Å resolution using synchrotron radiation and belong to the hexagonal space group $P6_322$, with unit-cell parameters a = 257.5, c = 443.5 Å. The unit cell contains two viral particles, with ten capsid viral protein monomers per crystallographic asymmetric unit.

1. Introduction

The development of viruses, such as the adeno-associated viruses (AAV), to deliver corrective genes into the cells or tissues of a target organism has gained momentum over the past few years. AAVs are members of the dependovirus genus of the *Parvoviridae* family, requiring a helper virus to cause a productive infection (Muzyczka & Berns, 2001). These viruses are non-pathogenic and non-toxic and can package and deliver foreign DNA into cells, making them attractive vectors for gene-therapy applications (Flotte & Carter, 1995). 11 serotypes of AAV have been identified in primates, with sequence homologies ranging from ~55 to 99% (Gao *et al.*, 2002; Mori *et al.*, 2004). These serotypes demonstrate varying cell-transduction efficiencies dictated by the amino-acid sequence of their capsid protein (Kaludov *et al.*, 2001; Walters *et al.*, 2001; Rabinowitz *et al.*, 2002; Gao *et al.*, 2002, 2003; Mori *et al.*, 2004; Burger *et al.*, 2004). For example, AAV8, which is an isolate from rhesus monkey tissue and largely homologous to the other AAVs, has a liver cell-transduction efficiency reported to be far greater than those of all others tested (Gao *et al.*, 2002). These observations have generated a need to understand the three-dimensional structure of the AAV capsids, aiming towards the improvement of their utilization for tissue-specific gene-therapy applications.

The AAV capsids contain 60 copies (in total) of three overlapping viral proteins, VP1–VP3, translated from the same mRNA, with the entire sequence of VP3 contained within VP2 and that of VP2 contained within VP1, which has a unique N-terminal domain. The three-dimensional structures of AAV2 (Xie *et al.*, 2002) and AAV4 (L. Govindasamy, E. Padron, N. Kaludov, R. McKenna, N. Muzyczka, J. Chiorini and M. Agbandje-McKenna, unpublished results) have been determined by X-ray crystallography. In these two AAV structures, plus all other structures determined for parvovirus capsids, only the overlapping C-terminal polypeptide sequence common to all the capsid proteins (~590 amino acids) is observed in a T = 1 icosahedral arrangement. Amino-acid sequences within this C-terminal domain determine the transduction phenotype of the AAVs. This paper reports the production, purification and preliminary X-ray crystallographic studies of the AAV8 viral capsid with the aim of obtaining a high-resolution structure for identifying the

specific variable capsid regions responsible for its preferential tropism for liver cells.

2. Materials and methods

2.1. Production and purification

A recombinant baculovirus encoding AAV8 capsid proteins VP1–VP3 was constructed using the Bac-to-Bac system (Gibco BRL). AAV2 capsid gene in pFBDVPm11 (Urabe *et al.*, 2002) was replaced by the respective gene encoding the AAV8 capsid derived from pAAV2/8 (Gao *et al.*, 2002). Similar mutations were introduced into 5′-noncoding and coding sequences to enable the expression of the AAV8 capsid gene in the insect-cell background (Urabe *et al.*, 2002). DH10Bac competent cells containing the baculovirus genome were transformed with pFastBac transfer plasmids containing the AAV component insert. Bacmid DNA purified from recombination-positive white colonies was transfected into Sf9 cells using TransIT Insecta reagent (Mirus). 3 d post-transfection, media containing baculovirus (pooled viral stock) were harvested and a plaque assay was conducted to prepare independent plaque isolates. Eight individual plaques were propagated to passage one (P1) to assay for the expression of the AAV8 capsid genes. A selected clone was propagated to P2, titered and used for large-scale rAAV preparations. Sf9 cells were cultivated by suspension culture in Erlenmeyer flasks at 300 K using Sf-900 II SFM media (Gibco/Invitrogen Corporation). AAV8 viral capsids were obtained by infecting the Sf9 insect cells at a multiplicity of infection of 5.0 plaque-forming units per cell with the recombinant virus, followed by incubation at 300 K for 72 h. Virus capsids were released from the Sf9 cells by repeated cycles (3×) of freezing and thawing prior to purification.

The initial step of the AAV8 capsid purification involved either an iodixanol step gradient [15–60%(*v*/*v*)] (prepared as described by Zolotukhin *et al.*, 1999) or a sucrose cushion [20%(*w*/*v*)] on the clarified lysate. Empty particles were harvested from the iodixanol gradient at the 25–40% junction and buffer-exchanged into 20 m*M* Tris–HCl pH 7.5 with 150 m*M* NaCl and 2 m*M* MgCl (buffer *A*) using Centriprep filters (Amicon Ultra, 30 000 MWCO). The sucrose-cushion procedure involved pelleting lysate (in 50 m*M* Tris–HCl pH 8.0, 150 m*M* NaCl, 0.2% Triton X-100) through a 20% sucrose cushion by ultracentrifugation at 45 000 rev min^{-1} for 3 h at 277 K. The pellet was resuspended in buffer *A*. The samples (25–45% buffer-exchanged iodixanol fraction or resuspended sucrose-cushion pellet) were further purified by a sucrose step gradient [5–40%(*w*/*v*)] by ultracentrifugation at 35 000 rev min^{-1} for 3 h at 277 K. A visible empty viral capsid band in the 20% sucrose fraction was collected and buffer-exchanged into buffer *A* containing 6% glycerol using Centricon filters (Amicon Centricons, 100 000 MWCO). The concentration of the sample, estimated by optical density measurements (using $E = 1.7$ for calculation in mg ml^{-1} units), was adjusted to 1.0–3.0 mg ml^{-1} for SDS–PAGE, electron microscopy and crystallization.

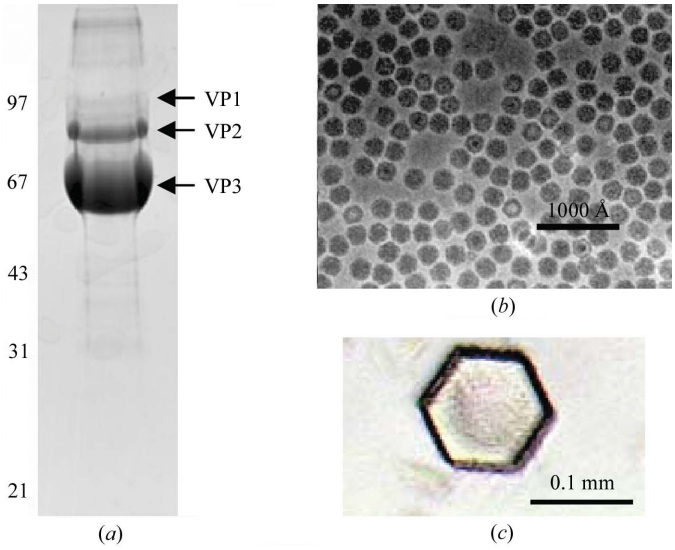

Figure 1
Purification and crystallization of AAV8 viral capsid. (*a*) SDS–PAGE of the purified sample. The three viral capsid proteins VP1, VP2 and VP3 are indicated with arrows and the positions of the molecular-weight markers are as given. (*b*) Negatively stained electron micrograph of the AAV8 capsids viewed at 50 000× on a Joel JEM-100CX II EM. The magnification bar represents 1000 Å. (*c*) Optical photograph of an AAV8 crystal in a hanging drop taken with a Zeiss Axioplan 2 microscope. Approximate crystal dimensions are 0.2 × 0.1 × 0.1 mm.

2.2. Electron microscopy

Purified AAV8 capsids were viewed using a Joel JEM-100CX II electron microscope (EM). 4 µl purified virus at an estimated concentration of 1.0 mg ml^{-1} was spotted onto a 400 mesh carbon-coated copper grid (Ted Pella Inc., Redding, CA, USA) for 1 min before blotting with filter paper (Whatman No. 5). The sample was then negatively stained with 4 µl 2% uranyl acetate for 15 s, blotted dry and viewed with the EM.

2.3. Crystallization, data collection and reduction

Crystallization conditions were screened by varying viral capsid concentration, pH and polyethylene glycol (PEG) 8000, glycerol, $MgCl_2$ and $LiSO_4$ concentrations in Tris–HCl and Bis-Tris buffers using the hanging-drop vapor-diffusion method (McPherson, 1982) in VDX 24-well plates with siliconized cover slips (Hampton Research, Laguna Niguel, CA, USA). Crystallization drops contained 2 µl sample and 2 µl precipitant solution and were equilibrated by vapor diffusion against 1 ml precipitant solution at room temperature.

For data collection, the crystals were flash-frozen with a cryoprotectant that consisted of precipitant solution with increased PEG 4000 and glycerol concentrations or by using Paratone-N (Hampton Research, Laguna Niguel, CA, USA). The X-ray diffraction data were collected at the 22-ID beamline of the South East Regional Collaborative Access Team (SER-CAT) facilities at the Advanced Photon Source, Argonne National Laboratory using a MAR300 CCD detector and at the F1 beamline at the Cornell High Energy Synchrotron Source (CHESS), Ithaca, NY, USA on an ADSC Quantum 4 CCD detector. Crystal-to-detector distances of 300–400 mm, oscillation angles of 0.2–0.3° and exposure times of 20 s (SER-CAT) and 2–4 min (CHESS) per image were used. The data were indexed and processed with *DENZO* and scaled and reduced with *SCALEPACK* (Otwinowski & Minor, 1997).

2.4. Calculation of particle orientation and position

The orientations of the virus particles in the crystal unit were determined with a self-rotation function using the *GLRF* program (Tong & Rossmann, 1997) computed with ∼10% of the observed data between 10.0 and 4.5 Å resolution as large terms at $\kappa = 72°$ (fivefold), 120° (threefold) and 180° (twofold). The particle position was inferred by packing considerations and confirmed using ten VP3 monomers from the previously determined viral capsid structure of AAV2 (Xie *et al.*, 2002) to calculate a cross-rotation and translation search using the *AMoRe* program (Navaza, 1994) with data in the 8.5–3.5 Å resolution range. The top solutions from the translation

function were refined using a rigid-body refinement option, FITTING, in *AMoRe* (Navaza, 1994). The initial model (of ten VP3 monomers) was positioned in the unit cell based on the molecular-replacement solution and crystallographic symmetry operators were applied to generate the two complete icosahedral particles in the unit cell. Phases were calculated from the model to 3.5 Å resolution in order to initiate structure determination by molecular replacement followed by refinement using the *CNS* program (Brünger *et al.*, 1998).

3. Results and discussion

3.1. Crystallization

The AAV8 viral capsids were purified through iodixanol and sucrose gradients and concentrated with filtration devices for structural studies by X-ray crystallography. The concentrated samples were run on SDS–PAGE (Fig. 1*a*) and viewed by an EM (Fig. 1*b*) to determine the purity and integrity of the particles prior to crystallization. The sample was judged to be >95% pure and the particles were observed to be intact.

Several crystals were obtained from the crystallization trials. The most consistent crystals grew using 100 m*M* Bis-Tris pH 6.5, 4.0–4.4% PEG 8000 and 6 or 20% glycerol. Thin plate-shaped and rod-shaped crystals were observed from these conditions (data not shown). Hexagonal shaped crystals were observed from drops that initially contained 20 m*M* Tris–HCl pH 7.5, 1.5% PEG 8000, 25 m*M* Li_2SO_4 and 6% glycerol (Fig. 1*c*).

3.2. Data collection, processing and scaling

X-ray diffraction data were collected from three different crystal forms. The thin plate-shaped crystals (~0.3 × 0.1 × 0.005 mm in size) were flash-frozen in a cryoprotectant solution containing 100 m*M* Tris–HCl pH 6.5, 4.0% PEG 4000 and 20% glycerol and X-ray diffraction data were collected at the F1 beamline at CHESS. The crystals diffracted to 3.5 Å resolution and were indexed in the orthorhombic space group, with unit-cell parameters $a = 247$, $b = 340$, $c = 1020$ Å. This data set is currently incomplete (data not shown). Diffraction data were collected on the rod-shaped crystals (~0.1 × 0.02 × 0.02 mm in size), also using the cryo-conditions described above, at F1. These crystals diffracted X-rays to 3.0 Å and also belong to the orthorhombic space group, with unit-cell parameters $a = 353$, $b = 367$, $c = 375$ Å. This data set is complete, but further utilization for structure determination is currently hindered by a high R_{sym} (defined in Table 1) (~22%) and weak overall $I/\sigma(I)$ (1.5) values for the measured reflections. The most complete X-ray diffraction data set with useful statistics has been collected from the hexagonal shaped crystals (~0.2 × 0.1 × 0.1 mm; Fig. 1*c*) at the 22-ID beamline at SER-CAT (Fig. 2). The crystals diffracted to 3.0 Å resolution, belong to the hexagonal Laue space group *P*622, with unit-cell parameters $a = 257.5$, $c = 443.5$ Å, and scale to an R_{sym} of 14.6% (Table 1). Inspection of the 00*l* reflections class (for $l = 2n$) resulted in the assignment of the space group as hexagonal $P6_322$. Although a sweep of ~25° of data was collected, only ~43% (accounting for ~11°) of the diffraction images collected were usable owing to radiation damage to the crystals during data collection. Statistics for this data set, utilized for molecular-replacement structure procedures, are reported in Table 1.

Table 1
Crystal data-collection and processing statistics.

Values in parentheses are for the highest resolution shell.

Wavelength (Å)	1.00
Space group	$P6_322$
Unit-cell parameters (Å)	$a = 257$, $b = 257$, $c = 443$
V_M† (Å^3 Da^{-1})	3.5
No. of observations	201131 (13772)
No. of unique reflections	114126 (7674)
Crystal mosaicity (°)	0.3
Resolution range (Å)	20–3.0 (3.11–3.00)
Completeness (%)	67 (45.8)
R_{sym}‡ (%)	14.6 (49.33)
Redundancy	1.8 (1.8)
$I/\sigma(I)$	4.8 (1.2)

† Matthews (1968). ‡ $R_{sym} = \sum|I_{hkl} - \langle I_{hkl}\rangle|/\sum\langle I\rangle \times 100$, where I_{hkl} is a single value of the measured intensity of the *hkl* reflection and $\langle I_{hkl}\rangle$ is the mean of all measured values of the intensity of the *hkl* reflections.

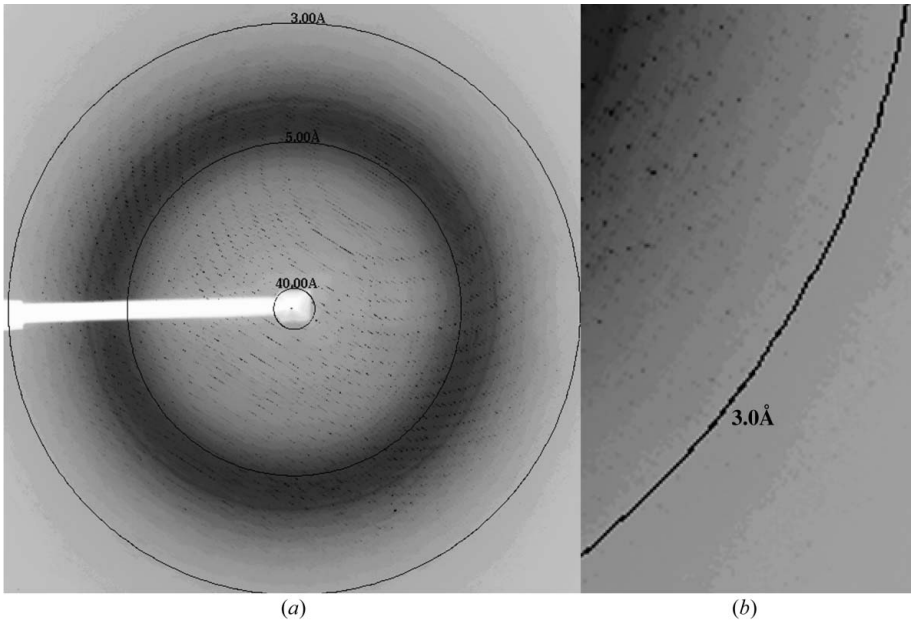

(*a*) (*b*)

Figure 2
Diffraction pattern for the hexagonal AAV8 viral capsid crystal. (*a*) Image of a typical 0.2° oscillation photograph. The concentric circles indicate resolution ranges of 40.0, 5.0 and 3.0 Å. (*b*) Close-up view of image in (*a*). Reflections are observed to at least 3.0 Å resolution.

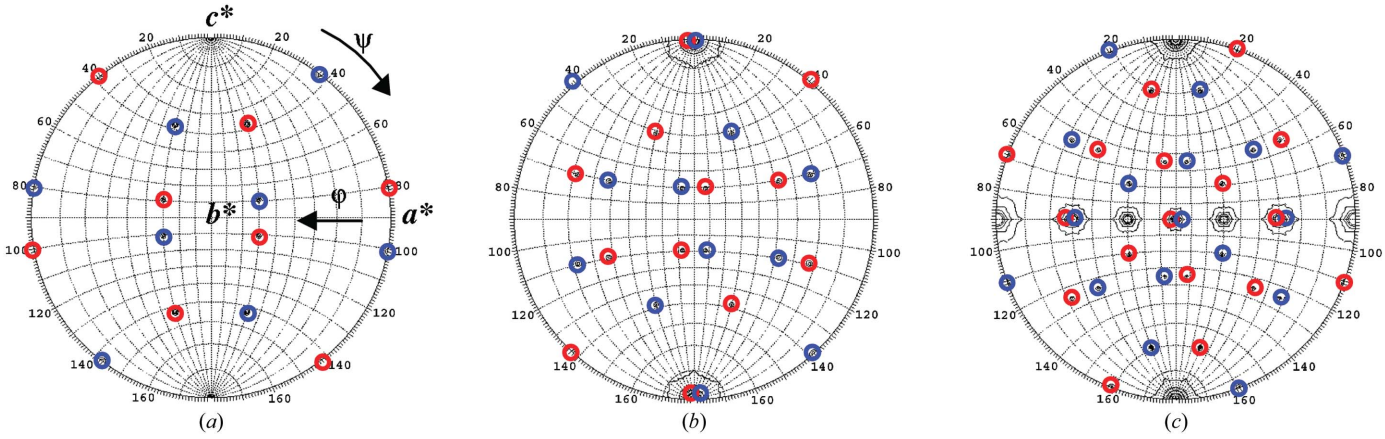

Figure 3
Self-rotation function for the AAV8 X-ray diffraction data, showing stereographic projections for $\kappa = 72^\circ$ (*a*), $\kappa = 120^\circ$ (*b*) and $\kappa = 180^\circ$ (*c*), searching for fivefold, threefold and twofold icosahedral symmetry elements, respectively. 10% of the observed data in the 10–4.5 Å resolution range were used as large terms, with a 120 Å radius of integration. The maps are all contoured starting at 1σ in steps of σ and the peaks belonging to each of the two viral capsids in the unit cell are circled the same color. The *a**, *b** and *c** axes are labeled.

3.3. Particle orientation and position

The hexagonal $P6_322$ unit-cell parameters and the molecular weight of the AAV8 viral capsid suggested that two viral particles can be packed into the unit cell, on the point-group symmetry operation 32, with ten VP monomers per asymmetric unit. The orientations of the two AAV8 particles in the crystal unit cell as determined by a self-rotation function (Tong & Rossmann, 1997) are shown in Fig. 3. Results of the self-rotation function clearly showed that the icosahedral threefold axes were coincident with the crystallographic threefold along the *c* unit-cell axis and that some of the icosahedral twofolds superimpose with the crystallographic twofold along unit-cell axis *a* (Fig. 3). Molecular-replacement procedures utilized ten AAV2 VP3 monomers in the viral asymmetric unit oriented and positioned by a cross-rotation and translation functions, respectively (Navaza, 1994). The initial search revealed unambiguous positions (1/3, 2/3, 1/4; 2/3, 1/3, 3/4), with an *R* factor ($\big||F_o| - |F_c|\big|/|F_o| \times 100$, where F_o and F_c are the observed and calculated structure factors, respectively) of 38% for data in the 15–3.5 Å resolution range after rigid-body refinement (FITTING in *AMoRe*). Initial rigid-body refinement with data in the 20–3.5 Å resolution range (∼73% completeness) using the *CNS* program (Brünger *et al.*, 1998) resulted in an *R* factor and R_{free} of 36.7%, with 5% of the data used as a test set for R_{free} calculation. The similarity of the *R* factor and R_{free} for virus structures stems from the high non-crystallographic icosahedral symmetry of their capsid. With this correct molecular-replacement solution available, the structure determination of AAV8 to 3.0 Å resolution using tenfold non-crystallographic symmetry to average the calculated electron-density maps should proceed without difficulties. This preliminary work represents a major step toward obtaining the essential high-resolution structural of AAV8. A crystal structure of AAV8 will facilitate the identification of the specific capsid regions responsible for its preferential tropism for liver cells to aid engineering of AAV vector capsids for improved gene-therapy applications in general.

The authors would like to thank the staff at the SER-CAT 22-ID beamline at the Advanced Photon Source, Argonne National Laboratory and the staff at the Cornell High Energy Synchrotron Source for assistance during X-ray diffraction data collection. Use of the Advanced Photon Source was supported by the US Department of Energy, Basic Energy Sciences, Office of Science under Contract No. W-31-109-Eng-38. We thank Dennifield Player (Anatomy and Cell Biology, University of Florida) for help with electron microscopy, Timothy Vaught (McKnight Brain Institute, Optical Microscopy Facility, University of Florida) for taking the optical photograph of the AAV8 crystals and Robbie Reutzel fo help with X-ray diffraction data collection. This project was funded by a University Scholars grant from the University of Florida to MDL and NIH projects P01 HL59412 and P01 HL51811 to NM, SZ and MA-M.

References

Burger, C., Gorbatyuk, O. S., Velardo, M. J., Peden, C. S., Williams, P., Zolotukhin, S., Reier, P. J., Mandel, R. J. & Muzyczka, N. (2004). *Mol. Ther.* **10**, 302–317.
Brünger, A. T., Adams, P. D., Clore, G. M., DeLano, W. L., Gros, P., Grosse-Kunstleve, R. W., Jiang, J.-S., Kuszewski, J., Nilges, M., Pannu, N. S., Read, R. J., Rice, L. M., Simonson, T. & Warren, G. L. (1998). *Acta Cryst.* D**54**, 905–921.
Flotte, T. R. & Carter, B. J. (1995). *Gene Ther.* **2**, 357–362.
Gao, G., Alvira, M. R., Somanathan, S., Lu, Y., Vandenberghe, L. H., Rux, J. J., Calcedo, R., Sanmiguel, J., Abbas, Z. & Wilson, J. M. (2003). *Proc. Natl Acad. Sci. USA*, **100**, 6081–6086.
Gao, G. P., Alvira, M. R., Wang, L., Calcedo, R., Johnston, J. & Wilson, J. M. (2002). *Proc. Natl Acad. Sci. USA*, **99**, 11854–11859.
Kaludov, N., Brown, K. E., Walters, R. W., Zabner, J. & Chiorini, J. A. (2001). *J. Virol.* **75**, 6884–6893.
McPherson, A. (1982). *Preparation and Analysis of Protein Crystals*, 1st ed., pp. 96–99. New York: Wiley & Sons.
Matthews, B. W. (1968). *J. Mol. Biol.* **33**, 491–497.
Mori, S., Wang, L., Takeuchi, T. & Kanda, T. (2004). *Virology*, **330**, 375–383.
Muzyczka, N. & Berns, K., (2001). *Fields Virology*, 4th ed., edited by D. M. Knipe & P. M. Howley, pp. 2327–2360. New York: Lippincott Williams & Wilkins.
Navaza, J. (1994). *Acta Cryst.* A**50**, 157–163.
Otwinowski, Z. & Minor, W. (1997). *Methods Enzymol.* **276**, 307–326.
Rabinowitz, J. E., Rolling, F., Li, C., Conrath, H., Xiao, W., Xiao, X. & Samulski, R. J. (2002). *J. Virol.* **76**, 791–801.
Tong, L. & Rossmann, M. G. (1997). *Methods Enzymol.* **276**, 594–611.
Urabe, M., Ding, C. & Kotin, R. M. (2002). *Hum. Gene Ther.* **13**, 1935–1943.
Walters, R., Yi, S. M., Keshavjee, S., Brown, K., Welsh, M., Chiorini, J. & Zabner, J. (2001). *J. Biol. Chem.* **276**, 20610–20616.
Xie, Q., Bu, W., Bhatia, S., Hare, J., Somasundaram, T., Azzi, A. & Chapman, M. S. (2002). *Proc. Natl Acad. Sci. USA*, **99**, 10405–10410.
Zolotukhin, S., Byrne, B. J., Mason, E., Zolotukhin, I., Potter, M., Chesnut, K., Summerford, C., Samulski, R. J. & Muzyczka, N. (1999). *Gene Ther.* **6**, 973–985.